Fast analytical estimation of the influence zone depth, its numerical verification and FEM accuracy testing

Pavel Kuklík[†]

Faculty of Civil Engineering, Czech Technical University in Prague, Czech Republic

Miroslav Brouček[‡]

Faculty of Civil Engineering, Czech Technical University in Prague, Czech Republic

Marie Kopáčková[‡†]

Faculty of Civil Engineering, Czech Technical University in Prague, Czech Republic

Abstract. For the calculation of foundation settlement it is recommended to take into account so called influence zone inside the subsoil bellow the foundation structure. Influence zone inside the subsoil is the region where the load has a substantial influence on the deformation of the soil skeleton. The soil skeleton is pre-consolidated or over consolidated due to the original geostatic stress state. An excavation changes the original geostatic stress state and it creates the space for the load transferred from upper structure. The theory of elastic layer in Westergard manner is selected for the vertical stress calculation. The depth of influence zone is calculated from the equality of the original geostatic stress and the new geostatic stress due to excavation combined with the vertical stress from the upper structure. Two close formulas are presented for the influence zone calculation. Using ADINA code we carried out several numerical examples to verify the proposed analytical formulas and to enhance their use in civil engineering practice. Otherwise, the FEM code accuracy can be control.

Keywords: pre-consolidation pressure; influence zone; Kantorovich method; fundamental solution layered subsoil; geostatic stress state; FEM.

1. Introduction

It is an experimentally confirmed fact that a soil substantially changes its material properties when subjected to external loading. Apart from that, the soil, when subjected to a certain loading history, has the ability to memorize the highest level of loading mathematically represented by over-consolidation ratio. In virgin state the soil deformability is relatively high. On the contrary,

---

† Associate Professor, Corresponding author, E-mail: kuklikpa@fsv.cvut.cz
‡ Ph.D. Student, E-mail: miroslav.broucek@fsv.cvut.cz
‡† Ph.D., E-mail: kopackova @math.cas.cz

following the unloading/reloading path shows almost negligible deformation until the highest stress state the soil has experienced ever before is reached (Bowles 1966, Kuklík *et al.* 1999, Janda *et al.* 2004, Fajman and Šejnoha 2007). When using standard recommendations (EUROCODE 7 1997) in the design, e.g., in the analysis of settlement of foundation subsoil, such a soil property is introduced by specifying the depth of influence zone. In order to obtain an analytical model reliable in describing the soil-structure interaction, it is crucial, to replace the usual semi-infinite subspace (Gecit 1981, Kukreti and Ko 1992, Davis and Selvadurai 1996, Mistrikova and Jendzelovsky 2007) by a layer of finite depth. The depth is determined by the magnitude of instantaneous loading and the level of previous consolidation (more in Kuklík and Kopáčková 2004).

2. The solution of elastic layer by means of the Kantorowich method

The aim of the analytical solution is to determine a deformation of an elastic layer in the vertical direction. The solution procedure builds upon neglecting the horizontal displacements similar to standard assumptions applied to the analysis of Westergard subspace. Clearly such an assumption results in a stiffer soil response thus providing an upper estimate of the depth of influence zone. The problem formulation is evident from Fig. 1. Referring to the Kantorovich method (details in Rektorys 1969, Shufrin and Eisenberger 2006) the distribution of the displacement field is searched in the form

$$w(x;y;z) = \sum_{j=1,3,5}^{\infty} w_j(x;y) \, \psi_j(z)$$

$$\psi_j(z) = \cos\frac{j\pi}{2H}z \tag{1}$$

where $\psi_j(z)$ is a known function of variable z and represents a complete set of base functions.

Let us calculate the components of the small strain tensor. Small strain tensor is the symmetrical part of the gradient matrix tensor. From (1) yields

$$\varepsilon_{xx} = 0, \quad \varepsilon_{yy} = 0, \quad \varepsilon_{zz} = \sum_{j=1,3,5}^{\infty} w_j \, \psi_{j,z}$$

$$\gamma_{xy} = 2\varepsilon_{xy} = 0, \ \gamma_{yz} = 2\varepsilon_{yz} = \sum_{j=1,3,5}^{\infty} w_{j,y} \, \psi_j, \ \gamma_{zx} = 2\varepsilon_{zx} = \sum_{j=1,3,5}^{\infty} w_{j,x} \, \psi_j \tag{2}$$
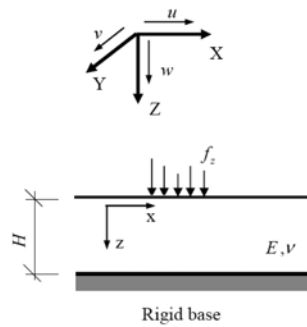

Fig. 1 Formulation of the elastic layer solution

Notation $\dfrac{\partial w_j}{\partial x} = w_{j,x}$ is used for partial derivative.

For stress-strain relation, general Hooke's law is adopted

$$\sigma_{xx} = \frac{v}{1-v}E_{oed}\sum_{j=1,3,5}^{\infty} w_j\,\psi_{j,z}, \quad \sigma_{yy} = \frac{v}{1-v}E_{oed}\sum_{j=1,3,5}^{\infty} w_j\,\psi_{j,z}, \quad \sigma_{zz} = E_{oed}\sum_{j=1,3,5}^{\infty} w_j\,\psi_{j,z}$$

$$\tau_{xy} = G\gamma_{xy} = 0, \quad \tau_{yz} = G\sum_{j=1,3,5}^{\infty} w_{j,y}\,\psi_j, \quad \tau_{zx} = G\sum_{j=1,3,5}^{\infty} w_{j,x}\,\psi_j \tag{3}$$

Symbols $E,\, v, E_{oed}, G$ represent known values of Young's modulus, Poisson's ratio, oedometric modulus, and shear modulus, respectively. Lagrange's principle of virtual work, general principle of equilibrium, is used in the following form

$$\int_{R^2}\left(\int_0^H\left(G\frac{\partial w}{\partial x}\frac{\partial \delta w}{\partial x} + G\frac{\partial w}{\partial y}\frac{\partial \delta w}{\partial y} + E_{oed}\frac{\partial w}{\partial z}\frac{\partial \delta w}{\partial z}\right)dz - f_z(x,y)\delta w(x,y,0)\right)dxdy = 0 \tag{4}$$

Since the virtual functions δw will be used in the same form as w, integrating equilibrium equation in vertical direction takes the form of infinite number of partial differential equations

$$-\Delta w_j(x,y) + (j\alpha)^2 w_j(x,y) = \frac{2}{GH}f_z(x,y), \quad j = 1,3,5,\dots$$

$$\alpha = \frac{\pi}{2H}\sqrt{\frac{E_{oed}}{G}} = \frac{\pi}{2H}\sqrt{\frac{2-2v}{1-2v}} \tag{5}$$

In the case of axisymetry or if the uniform load is acting on infinite strip the solution can be searched by solving system of ordinary differential equations. Otherwise, the strategy of convolution must be employed. Eq. (5), it generalizes of the known Pasternak solution of subsoil (see e.g., Filipich and Rosales 2002, Morfidis and Avramidis 2002, Celep and Demir 2007, Coşkun *et al.* 2008, Kotrasova 2009, Ma *et al.* 2009, Mistrikova and Jendzelovsky 2009).

2.1 Uniform load acting on an infinite strip

Denote the width of uniform load strip f_z by $2a$, i.e., $\Omega = \{[x,y]: -a < x < a,\ y \in R\}$. The solution $w(x,y,z)$ of (5) is independent on $y{:}w = w(x,z)$. Infinite number of the ordinary differential equations, together with the boundary and continuity conditions

$$\lim_{|x|\to\infty} w_j(x) = 0, \quad w_j \in C^1(R), j = 1,3,\dots$$

has the solution

$$w_j(x) = \begin{cases} A_0 + A_1\cosh(j\alpha x) & \text{for} \quad x \in <-a,\ a> \\ A_2\exp(-j\alpha|x|) & \text{for} \quad |x| > a \end{cases}$$

where

$$A_0 = \frac{2f_z}{GH}\left(\frac{1}{j\alpha}\right)^2$$

Unknown constants A_1, A_2 of integration result from the condition of continuity (of the displacement and the first derivative) in the points of $|x| = a$. Inserting these constants into above formula it provides

$$w_j(x) = \frac{2f_z}{GH}\left(\frac{1}{j\alpha}\right)^2 \cdot \begin{cases} 1 - \cosh(j\alpha x)\exp(-j\alpha a) & \text{for } |x| \le a \\ \exp(-j\alpha|x|)\sinh(j\alpha a) & \text{for } |x| > a \end{cases} \tag{6}$$

Hence, the function $w(x,z)$ being in the form of series

$$w(x,z) = \sum_{j=1,3,\dots} w_j(x)\cos\left(\frac{j\pi z}{2H}\right) \tag{7}$$

solves the problem. The component of the vertical stress function σ_{zz} is evaluated by differentiating $w(x,z)$ with respect to z by terms

$$\sigma_{zz}(x,z) = -E_{oed}\frac{\partial w}{\partial z}(x,z) = E_{oed}\sum_{j=1,3,\dots} \frac{j\pi}{2H}w_j(x)\sin\left(\frac{j\pi z}{2H}\right) =$$

$$= \frac{4f_z}{\pi}\sum_{j=1,3,\dots} \frac{1}{j}\sin\left(\frac{j\pi z}{2H}\right) \cdot \begin{cases} 1 - \cosh(j\alpha x)\exp(-j\alpha a) & \text{for } |x| \le a \\ \exp(-j\alpha|x|)\sinh(j\alpha a) & \text{for } |x| > a \end{cases}$$

All three series in the above formula can be summed (Gradschtein and Rizhik 1963). Finally, σ_{zz} can be written in the form

$$\sigma_{zz}(x,z) = f_z - \frac{f_z}{\pi}\left(\arctan\left(\frac{\sin(\pi z/2H)}{\sinh(\alpha(a-x))}\right) + \arctan\left(\frac{\sin(\pi z/2H)}{\sinh(\alpha(a+x))}\right)\right), \text{ for } |x| \le a$$

$$\sigma_{zz}(x,z) = \frac{f_z}{\pi}\left(\arctan\left(\frac{\sin(\pi z/2H)}{\sinh(\alpha(|x|-a))}\right) - \arctan\left(\frac{\sin(\pi z/2H)}{\sinh(\alpha(|x|+a))}\right)\right), \text{ for } |x| > a \tag{8}$$

3. The phenomenon of influence zone and the governing idea for its calculation

We introduce the subject consider the distribution of vertical stresses according to Fig. 2. Due to excavation to a certain depth h the original geostatic stress state, which sets the initial compaction of soil represented by the pre-consolidation pressure (Lewis and Schrefler 1998), the highest stress
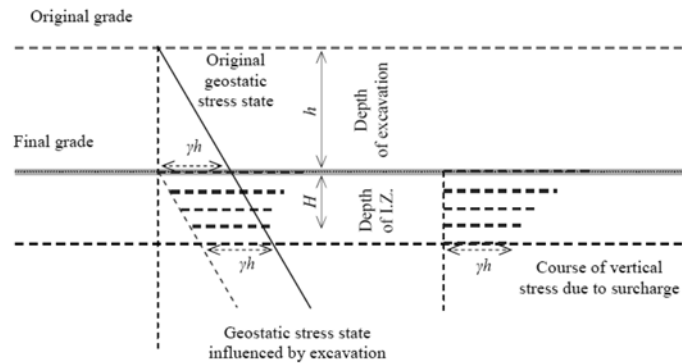

Fig. 2 The governing idea of the influence zone calculation

level soil records during the prior loading history, is reduced. Subsequent surcharge in the footing bottom gives further redistribution of the vertical stress. It is assumed that in the region where the vertical effective stress due to surcharge at the footing bottom combined with the reduced geostatic effective stress (by excavation) does not exceed the original geostatic effective stress the skeleton deformations are negligible. This condition, in our sense, describes the depth of the influence zone H (Daloglu and Ozgan 2004, Kuklík 2006).

3.1 Uniform load acting on an infinite strip

The stress function $\sigma_{zz}(x,z)$ for fixed $z \in <0, H>$ acquires its maximum at the point $x = 0$:

$$\max_{x \in R} \sigma_{zz}(x,z) = \sigma_{zz}(0,z) = f_z - \frac{f_z}{\pi}\arctan\left(\frac{\sin(\pi z/2H)}{\sinh \alpha a}\right) = \frac{2f_z}{\pi}\arctan\left(\frac{\sinh \alpha a}{\sin(\pi z/2H)}\right)$$

The function $\sigma_{zz}(0,z)$ decreases with increasing z. The maximum of the stress function at the bottom of the influence zone depth is

$$\sigma_{zz}(0,H) = \frac{2f_z}{\pi}\arctan \sinh \alpha a \tag{9}$$

The influence zone depth is estimated by means of the quality

$$\sigma_{zz}(0,H) = \gamma h \tag{10}$$

where γ is the specific weight of soil and h is the depth of excavation.

Comparing last two identities we obtain

$$\frac{\gamma h}{f_z} = \frac{2}{\pi}\arctan \sinh \alpha a$$

Denoting

$$\beta = \frac{2\alpha a}{\pi} = \frac{a}{H}\sqrt{\frac{2 - 2v}{1 - 2v}}, \quad F_{strip}(\beta) = \frac{2}{\pi}\arctan\left(\sinh\frac{\beta\pi}{2}\right)$$

The above identities give the equation

$$\frac{\gamma h}{f_z} = F_{strip}(\beta)$$

Eliminating influence zone finally yields

$$H = \frac{\pi a}{2}\sqrt{\frac{2 - 2v}{1 - 2v}}\frac{1}{\sinh^{-1}\left(\tan\frac{\pi \gamma h}{2f_z}\right)} = \frac{\pi(2a)}{4}\sqrt{\frac{2 - 2v}{1 - 2v}}\frac{1}{\sinh^{-1}\left(\tan\frac{\pi \gamma h}{2f_z}\right)} \tag{11}$$

This closed formula can be effectively used in civil engineering practice. Now we give several comments on derived identity. At first, the influence zone is proportional to the strip load width $2a$. Secondly, the influence zone doesn't depend on Young's modulus, but significant role plays Poisson's ratio. Overloading of the excavation geostatic stress state $f_z/\gamma h$ is the third parameter to be taken into account. All this statements are highlighted in following Fig. 3.
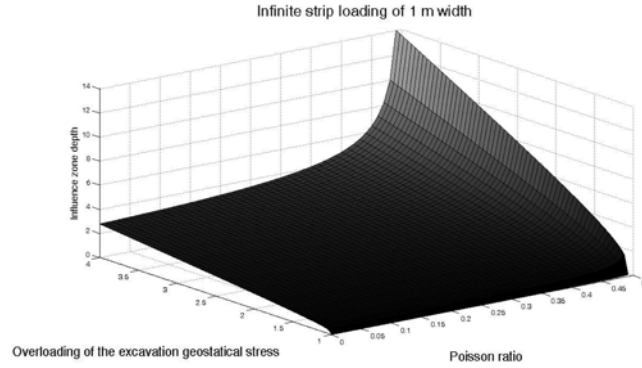
Fig. 3 Progress of influence zone depth of the 1m wide strip

3.2 Uniform load acting on straight line

If the width $2a$ decreases to 0 and the uniform load f_z increases

$$f_z = \frac{f_z^l}{2a}$$

The limit value $\sigma_{zz}(0,z)$ at the point $[0,y,z]$ for $a \rightarrow 0$ is obtaining by limit process using the l'Hospital's rule

$$\sigma_{zz}^l(0,z) = \lim_{a \to 0} \sigma_{zz}(0,z) = \frac{f_z^l}{\pi} \lim_{a \to 0} \frac{1}{a} \arctan\left(\frac{\sinh(\alpha a)}{\sin(\pi z/2H)}\right) =$$

$$= \frac{f_z^l}{\pi} \lim_{a \to 0} \frac{\cosh(\alpha a)\,\alpha\sin(\pi z/2H)}{\sin^2(\pi z/2H) + \sinh^2(\alpha a)} = \frac{f_z^l \alpha}{\pi\sin(\pi z/2H)} \quad \text{for} \quad z > 0$$

(12)

The very important value of the stress function $\sigma_{zz}(0,H)$ for uniform load acting in line is given in the form

$$\sigma_{zz}^l(0,H) = \frac{f_z^l \alpha}{\pi} = \frac{f_z^l}{2H}\sqrt{\frac{2-2\nu}{1-2\nu}}$$

(13)

From above equation immediately yields another usable formula

$$H = \frac{f_z^l}{2\gamma h}\sqrt{\frac{2-2\nu}{1-2\nu}}$$

(14)

4. Verification using FEM

The aim of this chapter is to provide results obtained from finite element (FE) analysis and compare them with results obtained from the presented theory of elastic layer. The line load and the infinite strip load were selected for comparison. The values of $\sigma_{zz}(0,H)$ were compared. The influence of the FE mesh as well as model width and type of FE is evaluated.

4.1 Summary of analytical results

Let us first remind derived formulas for $\sigma_{zz}(0, H)$ in case of straight line load and infinite strip load.

1) Line load

$$\sigma_{zz}^l(0, H) = \frac{1}{2H} f_z^l \sqrt{\frac{2 - 2\nu}{1 - 2\nu}}$$

Where H: depth of influence zone,
f_z^l: value of the line load,
ν : Poisson's ratio.

2) Infinite strip load

$$\sigma_{zz}(0, H) = \frac{2f_z}{\pi} \arctan \sinh \alpha a$$

Where: H: depth of influence zone,
f_z : value of the strip load,
ν : Poisson's ratio,
a : half of the strip width,
$\alpha: \alpha = \frac{\pi}{2H} \sqrt{\frac{2 - 2\nu}{1 - 2\nu}}$

4.2 Finite element method (FEM)

For the FEM analysis were used following assumptions.
• 1 degree of freedom for nodes (z-direction)
• Plain strain
• Isotropic elastic material
• Symmetry-only one half of the model
• Software ADINA (Automatic Dynamic Incremental Non-linear Analysis)

The influences of the model width, mesh shape and type of the used finite elements on the results are commented in the following parts of the chapter.

4.2.1 Tested example
The tested example has following details:
• Line load $f_z^l = 100000$ kN/m
• Infinite strip load $f_z = 100000$ kN/m^2 for $a = 0,5$ m; $f_z = 50000$ kN/m^2 for $a = 1,0$ m; etc.
• Depth of influence zone $H = 5$ m
• $E = 75$ GPa
• ν varies from 0,05 to 0,4
• Model width $B = 30$ m (15 m using symmetry)
An unreal magnitude of load was used to reach sufficient digital output in the computer code.
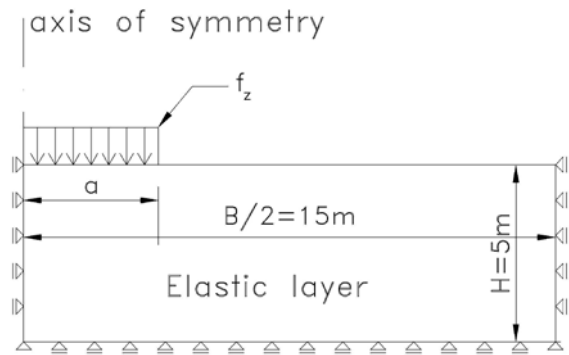The scheme of the example can be seen on the following figure.

Fig. 4 Scheme of the tested example

4.2.2 Numerical results

The following Fig. 5 presents analytical and numerical results for $a = 0\,\text{m} - 8\,\text{m}$, i.e., from line load to very wide strip. The presented results show very good agreement. The differences are smaller than 0,1% for this range of Poisson's ratio (from 0.05 to 0.4). The differences rise as the Poisson's ratio get closer to 0,5. Table 1 and Table 2 show the base data for graph on Fig. 5 and Fig. 6. Dashed lines called ANA 0,05 – ANA 0,4 are showing analytical results. On the next Fig. 7

Table 1 Numerical results

1/2 uniform load width (m)	0	0.5	1	2	4	8
Poisson's ratio	$\sigma_{zz}(0, H)$ (kPa)					
0.05	14531.1	14412.0	14053.9	12853.8	9959.04	6044.0
0.15	15585.0	15437.8	15000.4	13565.1	10269.9	6091.8
0.25	17322.0	17118.7	16528.5	14661.8	10702.9	6147.7
0.3	18709.0	18453.2	17720.4	15472.4	10988.6	6177.8
0.35	20818.0	20464.7	19479.0	16596.9	11339.0	6207.5
0.4	24495.8	23922.6	22388.4	18273.6	11767.9	6233.1
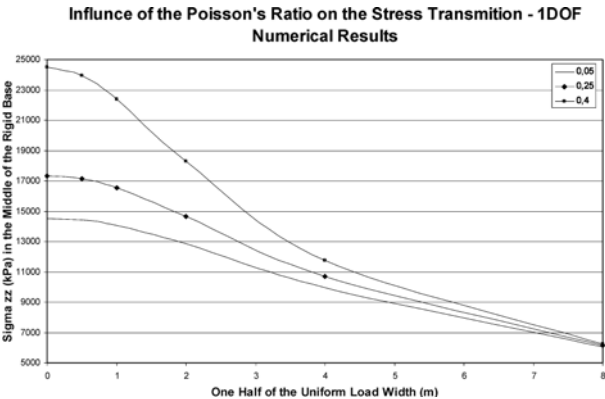
Fig. 5 Numerical results

Table 2 Analytical results

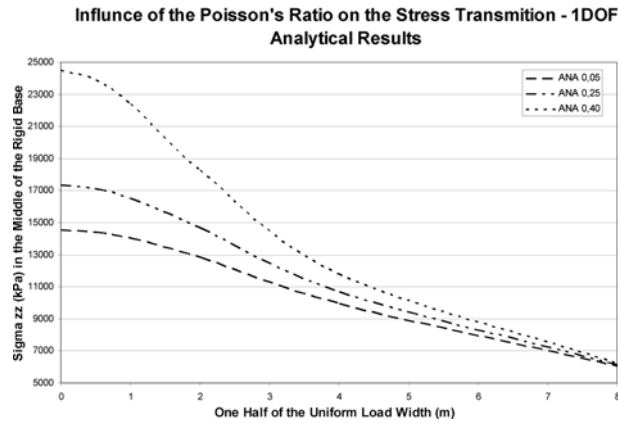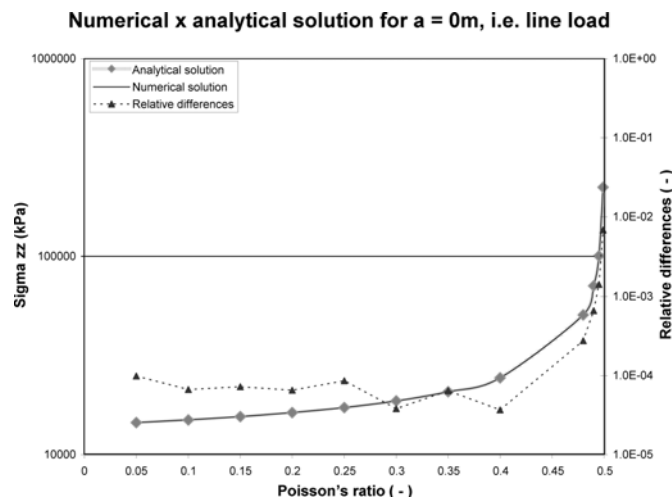| 1/2 uniform load width (m)	0	0.5	1	2	4	8
Poisson's ratio	$\sigma_{zz}\,(0, H)$ (kPa)					
0.05	14529.7	14405.1	14049.9	12851.1	9958.2	6043.6
0.15	15583.9	15430.5	14996.2	13562.5	10269.1	6091.6
0.25	17320.5	17110.7	16524.1	14659.3	10702.4	6147.6
0.3	18708.3	18444.7	17715.8	15470.0	10988.2	6177.8
0.35	20816.7	20455.3	19474.1	16594.7	11338.6	6207.5
0.4	24494.9	23912.0	22383.3	18271.7	11767.7	6233.1

Fig. 6 Analytical results

Fig. 7 Analytical *x* numerical results and their relative differences

the numerical and analytical solution for straight line load is plotted. On the right vertical axis are plotted the relative differences between the solutions. The differences are smaller than 0,1% for

Poisson's ratio smaller than 0,49. Both vertical axes in this chart are in logarithmic scale. In all presented results we keep the geotechnical convention in the stress values, i.e., positive stress value means pressure while negative stress value is tension.

4.3 Influence of the model width

The influence of the model width on the value of σ_{zz} (0, H) was tested on the 7 node elements. Number of the FE in the mesh remains unchanged for the comparison purposes. However in one case the mesh was designed denser in order to verify the conclusions made. The influence zone depth was kept on 5 m. The analytical solution gives the σ_{zz} (0, H) value 18 706 kPa and the results from numerical analysis are in Table 3.

Table 3 Numerical results for varying model width

Number of DOF	Number of FE	Model width (m)	σ_{zz} (kPa)	Relative difference (%)
2259	724	30	18699	−0.05
2259	724	20	18705	−0.02
2259	724	10	18919	1.13
5763	1879	10	18918	1.12
2259	724	40	18691	−0.09

Table 4 Numerical results for varying FE mesh and types of FE

| Mesh type	FE type	FE area (m^2)	Number of DOF	Number of FEM	σ_{zz} (kPa)	Relative diff. (%)
TYPE 1	9-NODE QUAD	0.06875	1559	374	18665	−0.23
	7-NODE TRIANGL	0.034375	2259	724	18678	−0.16
	4-NODE QUAD	0.06875	406	374	18621	−0.47
	3-NODE TRIANGL	0.034375	406	724	18765	0.31
TYPE 2	9-NODE QUAD	0.0187	1559	374	18687	−0.11
	7-NODE TRIANGL	0.00935	2259	724	18694	−0.08
	4-NODE QUAD	0.0187	406	374	18657	−0.27
	3-NODE TRIANGL	0.00935	406	724	18757	0.26
TYPE 3	9-NODE QUAD	0.0125	1559	374	18698	−0.06
	7-NODE TRIANGL	0.00625	2259	724	18699	−0.05
	4-NODE QUAD	0.0125	406	374	18689	−0.10
	3-NODE TRIANGL	0.00625	406	724	18912	1.09
TYPE 4	9-NODE QUAD	0.0825	3731	900	18638	−0.38
	7-NODE TRIANGL	0.04125	5531	1800	18659	−0.26
	4-NODE QUAD	0.0825	966	900	18568	−0.75
	3-NODE TRIANGL	0.04125	966	1800	18817	0.58
TYPE 5	9-NODE QUAD	0.01155	3709	900	18691	−0.09
	7-NODE TRIANGL	0.005775	5455	1773	18697	−0.06
	4-NODE QUAD	0.01155	955	900	18672	−0.20
	3-NODE TRIANGL	0.005775	955	1773	18729	0.11
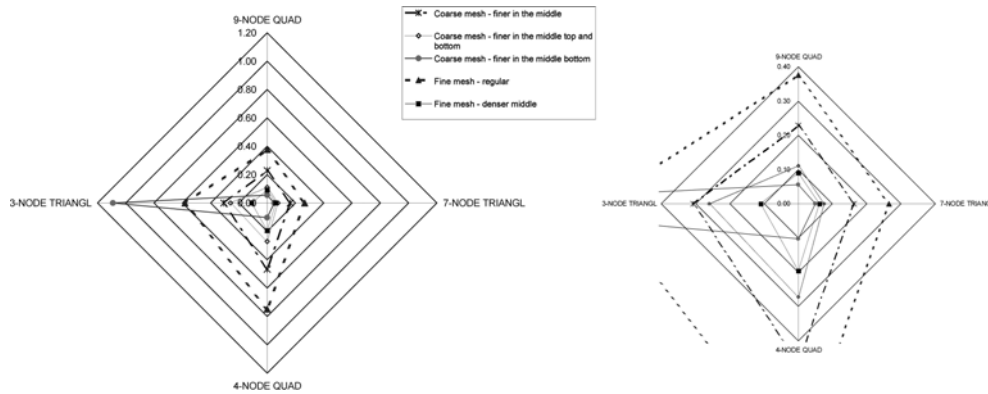
Fig. 8 Relative differences for different types of FE mesh and FE type and detail
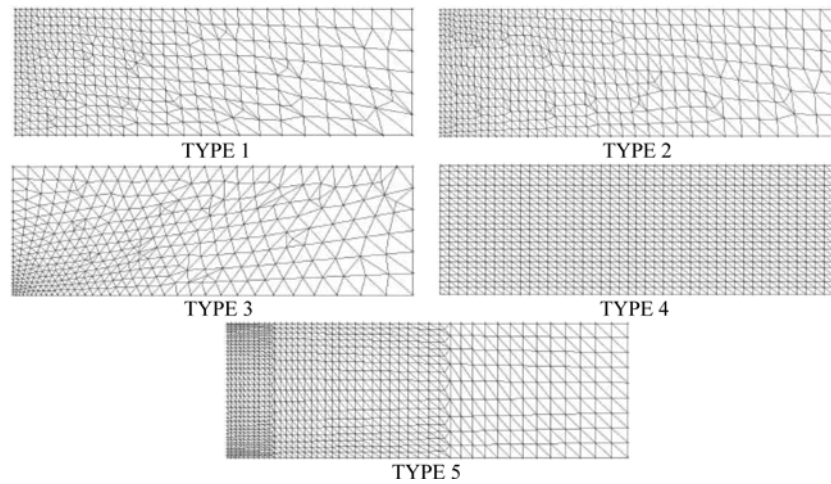

Fig. 9 Types of FE mesh and FE type

4.4 Influence of the FE mesh shape and type of FE

The influence was tested on the line load case. The value of the load $f_0 = 100000 \, \text{kN/m}$ and the Poisson's ratio $\nu = 0.3$. Four types of FE were tested, i.e., triangle with 7 and 3 nodes and quad with 9 and 4 nodes. The width of the model remains 30 m. Five different settings of the FE mesh were tested. Three types had coarse mesh with different points of densification. Two types had fine mesh. The results are in Table 4 and the relative differences are also plotted in Fig. 8. The FE meshes are introduced in Fig. 9. The FE area belongs to the finite element at the bottom from which we obtain the stress value.

5. Conclusions

The FEM numerical analysis results have proved to be in a good agreement with presented analytical solution. Although the relative differences are dependent on the chosen type of the FE

and the shape of FE mesh, they do not exceed 2% of the analytically estimated values. From the practical point of view, such value is negligible compare to the uncertainties in the soil parameters.

From the obtained results can be concluded that optimal width of the model B is B $\geq$ 4H, i.e., model width equals four times influence zone depth. Otherwise (B < 4H) the numerical response is a little bit stiffer, as it can be seen in Table 3. From the results is also clear that for too narrow model increasing number of FE (denser mesh) do not increase the accuracy of results significantly.

Seven node triangle and nine node quad seemed to be the most suitable types of FE. Unlike the 4, 7 and 9 node FE the 3 node elements give higher values of stress than analytical solution. From the Fig. 7 it is evident that some FE mesh settings are more suitable for some FE types. For example type 3 mesh gives very good results for 7 and 9 node element but less accurate results for 3 nodes FE. It is also clear that the choosing the appropriate type of mesh will improve the results accuracy more than just creation of denser mesh even in case as simple as this one (elastic solution, plane strain, no contact, etc.).

The derived formulas for influence zone depth present a useful tool for any numerical analysis of settlement of strip footings. The differences between results from FEM numerical analysis and presented analytical solution are negligible. The derived formulas can be considered as verified.

Acknowledgements

References

Bowles, J.E. (1966), *Foundation Analysis and Design*, McGraw-Hill, New York.
Celep, Z. and Demir, F. (2007), "Symmetrically loaded beam on a two parameter tensionless foundation", *Struct. Eng. Mech.*, **27**(5), 554-574.
Coşkun, I., Engin, H. and Ozmutlu, A. (2008), "Response of a finite beam on tensionless Pasternak foundation under symmetric and asymmetric loading", *Struct. Eng. Mech.*, **30**(1), 21-36.
Daloglu, A.T. and Ozgan, K. (2004), "The effective depth of soil stratum for plates resting on elastic foundation", *Struct. Eng. Mech.*, **18**(2), 263-276.
Davis, R.O. and Selvadurai, A.P.S. (1996), *Elasticity and Geomechanics,* Cambridge University Press.
EUROCODE 7 (1997), *General Rules-spread Foundations, Geotechnical Design*, Prague.
Fajman, P. and Šejnoha, J. (2007), "A simplified approach to time-dependent subsoil-structure interaction", *Comput. Struct.*, **85**, 1514-1523.
Filipich, C.P. and Rosales, M.B. (2002), "A further study about the behaviour of foundation piles and beams in a Winkler-Pasternak soil", *Int. J. Mech. Sci.*, **44**, 21-36.
Gecit, M.R. (1981), "Axisymmetric contact problem for an elastic layer and an elastic foundation", *Int. J. Eng. Sci.*, **19**(6), 747-755.
Gradschtein, I.S. and Rizhik, I.M. (1963), *Tables of Integrals, Sums, Series and Product*, (in Russian) Moscow.
Janda, T., Kuklík, P. and Šejnoha, M. (2004), "Mixed experimental and numerical approach to evaluation of material parameters of clayey soils", *Int. J. Geomech.*, **4**(3), 199-206.
Kotrasová, K. (2009), "Influence of category of sub-soil on liquid storage circular tanks during earthquake", 12th International Scientific Conference, 2009, Brno Czech Republic.
Kuklík, P. (2006), "Several comments on influence zone depth progress in deep hole foundations", *Proceedings of the GeoShanghai Conference,* 2006, Reston.

Kuklík, P., Šejnoha, M. and Mareš, J. (1999), "The structural strength of soil from the isotropic consolidation point of view", *Proceedings of APCOM 99*, Singapore.

Kuklík, P.M. and Kopáèková, M. (2004), "Comparison of elastic layer solution with Boussinesq half space solution", *Stavební Obzor*, **6**, 171-175. (in Czech)

Kukreti, A.R. and Ko, M.G. (1992), "Analysis of rectangular plate resting on an elastic half space using an energy approach", *Appl. Math. Model.*, **16**(7), 338-356.

Lewis, R.W. and Schrefler, B.A. (1998), *The Finite Element Method in the Static and Dynamic Deformation and Consolidation of Porous Media*, John Wiley & Sons Ltd., Chichester.

Ma, X., Butterworth, J.W. and Clinton, G.C. (2009), "Static analysis of an infinite beam resting on a tensionless Pasternak foundation", *Eur. J. Mech. A-Solid*, **28**(4), 697-703.

Mistrikova, Z. and Jendzelovsky, N. (2007) "Sub soil modeling and its influence on foundation slab deformation and stress state inside the slab", *Civil Environ. Eng.*, **3**(2), 139-148. (in Slovak)

Mistrikova, Z. and Jendzelovsky, N. (2009) "Soil - axisymmetric slab interaction for different models of subsoil", *Civil Environ. Eng.*, **5**(1), 18-28. (in Slovak)

Morfidis, K. and Avramidis, I.E. (2002), "Formulation of a generalized beam element on a two-parameter elastic foundation with semi-rigid connections and rigid offsets", *Comput. Struct.*, **80**(25), 1919-1934.

Rektorys, K. (1995), *Survey of Applicable Mathematics*, ILIFFE Books: London.

Shufrin, I. and Eisenberger, M. (2006), "In-plane vibrations of rectangular plates with rectangular cutouts", *Proceedings of the EPMESC X.*, Sanya, China.